Chemical routes to materials



Influence of multi-walled carbon nanotubes on the fracture response and phase distribution of metakaolin-based potassium geopolymers

Jiaxin Chen¹ and Ange-Therese Akono^{1,2,*}

Received: 11 March 2021 Accepted: 18 September 2021

© The Author(s), under exclusive licence to Springer Science+Business Media, LLC, part of Springer Nature 2021

ABSTRACT

This research investigated the effects of multi-walled carbon nanotubes (MWCNTs) on the chemistry, microstructure, phase distribution, and fracture response of potassium-based metakaolin geopolymers at the microscopic scale. We formulated novel protocols to cast geopolymers reinforced with 0.3, 0.6, and 1.5 wt% MWCNTs. We studied the chemistry using XRD, FTIR, and solid state ²⁹Si NMR. We characterized the microstructure and dispersion state of MWCNTs geopolymers using microscopic imaging and high-resolution scanning electron microscopy. We assessed the fracture behavior and mechanical properties using scratch tests and indentation tests. We used cluster analysis of indentation results to study the phase distribution. MWCNTs were well dispersed with an average accumulated area less than 8.9 µm². XRD showed that MWCNTs preserved the amorphous phase. NMR showed that the addition of MWCNTs decreased Q⁴(Al2) fraction, but increased Q⁴(Al3) fraction. We observed a densification of the microstructure and a reduction in porosity. The microstructure showed that MWCNTs acted as bridges for fracture surfaces and connections for pores. The addition of 0.6 wt% MWCNTs increased the strength by 3.2%, and stiffness by 11.1%. Meanwhile, the addition of 1.5 wt% MWCNTs addition increased the fracture toughness by 10.5%. An inner strengthening effect was observed as MWCNTs reduced the microporosity, resulting in an increase in the indentation modulus and hardness for the dominant microphase. Therefore, MWCNTs promote the geopolymerization reaction, strengthen the geopolymer skeleton, affect the pore structure, and improve mechanical characteristics.

Handling Editor: Yaroslava Yingling.

Address correspondence to E-mail: ange-therese.akono@northwestern.edu

https://doi.org/10.1007/s10853-021-06547-0

Published online: 11 October 2021



¹Department of Civil and Environmental Engineering, Northwestern University, Evanston, IL, USA

²Department of Mechanical Engineering, Northwestern University, Evanston, IL, USA

GRAPHICAL ABSTRACT

Introduction

Geopolymers are amorphous aluminosilicate materials composed of cross-linked alumina AlO₄ and silica SiO₂ tetrahedra that form polysialates [1]. Geopolymers have become popular in recent years as an ecofriendly alternative to cement given their low carbon footprint [1–8]. When the source of aluminosilicate is synthetic metakaolin, the geopolymer is referred to as a metakaolin-based geopolymer, which is pure and considered to be a "model system" [9, 10]. Metakaolin-based geopolymers generally have a faster setting time compared to ordinary Portland cement [3, 4] and have excellent durability in extreme environments [11, 12, 29]. They have also shown excellent performance in terms of high compressive strength and low thermal conductivity [4], low shrinkage [13, 14], high acid resistance, and high fire resistance [15]. There are many potential applications for metakaolin-geopolymers, such as next-generation alternative construction materials [16], three-dimensional (3-D) printing applications [17, 18], and sensing structures [19]. There has been an increased focus on geopolymer nanocomposites for "smart" infrastructures. An emerging class of nanomaterials for geopolymers are carbon-based nanomaterials like multi-walled carbon nanotubes (MWCNTs), which are characterized by their excellent thermal conductivity, enhanced fire performance, strength, and light weight [20–26].

Dispersion of high concentration levels of MWCNTs in the geopolymer matrix remains a challenge due to the strong van der Waals interactions leading to MWCNTs clusters or bundles [24, 27–31]. Researchers have used surface treatment [16, 29], ultrasonication [32], and superplasticizers [32] to assist dispersion. However, most methods have led to a decrease in mechanical properties when dispersing high concentration levels of MWCNTs. Using superplasticizers and 20-min ultrasonication to disperse MWCNTs, Abbasi et al. [32] found that at 0.5 wt% MWCNTs, the metakaolin geopolymer's compressive strength increased by 32% and flexural strength by 28%. However, they observed that there was a small decrease in both compressive strength and flexural strength with a the high concentration level of 1.0 wt% MWCNTs. High concentration level of MWCNTs (1.0 wt%) in geopolymers has also been shown to increase the electrical conductivity by 194% [16], which demonstrates their potential for application in "smart" infrastructures. Saafi et al. [16] used



surfactant and 120-min sonication to create up to 1.0 wt% MWCNTs fly ash geopolymers. They found that the optimum amount of MWCNTs for fly ash geopolymers was 0.5 wt% and observed a decrease in terms of flexural strength, Young's modulus, and flexural toughness with the addition of 1.0 wt% MWCNTs. Yuan *et al.* [33] mixed metakaolin with MWCNTs in ethanol with zirconia balls for 24 hours and achieved high concentration levels of 0.5–5.0 wt%. They determined that 3.0 wt% MWCNTs increased the fracture toughness by 38.5% and elastic modulus by 29.6%. However, a decrease in mechanical properties was also observed in their study. Therefore, a new dispersion method for MWCNTs needs to be developed.

The influence of MWCNTs on the mechanical properties of geopolymers also requires further studies. Studies of the influence of MWCNTs on the fracture response of nanocomposites have been studied before, for polymers. Gholami and Khayamdar et al. studied the effects by MWCNTs on adhesives [36], polymer adhesive joints [34, 38], and epoxy adhesives [37]. MWCNTs are popular for enhancing the fracture properties of polymer composites [35] and also applied for construction materials [19, 39, 40]. However, there are few fracture studies on metakaolin geopolymer systems. Rovnanik et al. [40] investigated the fracture performance of fly-ash geopolymers with MWCNTs. However, few studies have investigated the effects of MWCNTs on the fracture performance of metakaolin-based geopolymers. Yuan et al. [33] investigated the enhancement effect of MWCNTs on fracture toughness of metakaolin-based geopolymers at the macroscale. However, the fracture toughness value of their reference plain geopolymer was low compared to other studies such as [21, 41, 42]. The effects of MWCNTs on the enhancement of fracture resistance requires further investigation.

The influence of MWCNTs on the microstructure of the metakaolin-based geopolymer matrix remains unclear. For slag-based geopolymers, Rovnanik *et al.* [40] and Khater *et al.* [43] found that the MWCNTs decreased the porosity, which resulted in an increase in the mechanical properties. For metakaolin-based geopolymers, da Luz *et al.* [29], Abbasi *et al.* [32], and Yuan *et al.* [33] found that in terms of microstructure, MWCNTs acted as bridges, increasing the bridging between geopolymer matrix. However, few qualitative analyses have investigated this microstructure

bridging effect. Abbasi *et al.* [32] and da Luz *et al.* [29] investigated the chemical effects of metakaolin compared with a plain geopolymer using Fourier-transform infrared spectroscopy (FTIR) analysis. Yuan *et al.* [33] studied the effects of temperature on a 3 wt% MWCNTs geopolymer. However, the chemical effects of different concentration levels of MWCNTs have not yet been investigated.

Rheology is another important factor for workability and potential 3-D printing applications. Da Luz *et al.* [29] found that the addition of MWCNTs did not influence the rheology of metakaolin-based geopolymers. However, our extended study on a wider range of concentration levels of MWCNTs revealed different results from their conclusions.

Our research objective is to understand the influence of high concentration levels of MWCNTs on the rheology of fresh geopolymer paste, the hardened properties including geopolymerization phase distribution, fracture resistance, and on the nanostructure and microstructure of hardened geopolymer matrices. This study combined rheology characterization, chemical characterization, and depth-sensing mechanical characterization with cluster analysis. In addition to characterization, we applied image analysis with a large dataset to characterize the MWCNTs dispersion state. To this end, we employed grid indentation to quantitatively evaluate the strengthening effects and characterize the microstructure effects of metakaolin-based potassium geopolymers reinforced with MWCNTs at different concentration levels. We obtained the phase distribution based on the grid indentation results to study the effects of the MWCNTs on the microstructure of the geopolymer matrix. Furthermore, using statistical analysis, we evaluated the phase distribution of geopolymer nanocomposites to study the influence of MWCNTs on the mechanical micro-constituents. Moreover, to understand the chemical effect of MWCNTs, we performed XRD, FTIR, and NMR analysis. In addition, we characterized the rheological properties of our geopolymer nanocomposites to assess their workability and potential for 3-D printing applications. Table 1 introduces the mathematical notations used in this study.



Table 1 Nomenclature

Symbol	Definition	Symbol	Definition
$\overline{A_c}$	Contact area	μ	Mean value
F_T	Horizontal force	η_p	Plastic viscosity
γ	Shear rate	$\stackrel{'}{P}$	Vertical force
H	Indentation hardness	ϕ	Porosity
h	Indentation depth	R^2	Coefficient of determination
K_c	Fracture toughness	s	Standard derivation
M	Indentation modulus	$ au_0$	Yield shear stress
MWCNTs	Multi-walled carbon nanotubes	τ	Shear stress

Materials and methods

Materials

To synthesize the metakaolin-based potassium geopolymer nanocomposites, we used raw materials including potassium hydroxide (Thermo Fisher Scientific, Waltham, MA, USA), fumed silica (Wacker, Munich, Germany), deionized water, and metakaolin (BASF, Ludwigshafen, Germany) along MWCNTs (Cheaptubes, Grafton, VT, USA). The chemical composition for the reference geopolymer was $K_2O \cdot Al_2O_3 \cdot 4SiO_2 \cdot 11H_2O$. The fumed silica had a particle size of 70 nm and a surface area of 300 $m^2 \cdot g^{-1}$. The MWCNTs had an outer diameter of < 8nm, an inner diameter of 2-5 nm, a length of 10-30 μ m, and a specific surface area of 500 m² · g⁻¹. Scanning electron microscope (SEM) and X-ray diffraction (XRD) of MWCNTs are shown in Fig. 1. Xray peaks exist at the diffraction angels (2 θ) of 26.0°, 42.9°, and 44.1°, which can be assigned to the C(002) and C(100) reflection of the highly ordered graphitic structure of carbon atoms [48–50]. We manufactured four types of geopolymer nanocomposites as shown in Table 2. The plain geopolymer without MWCNTs named KCT0.0. The was geopolymer

Figure 1 a SEM of Raw

MWCNTs; **b** XRD of Raw

MWCNTs in this study.

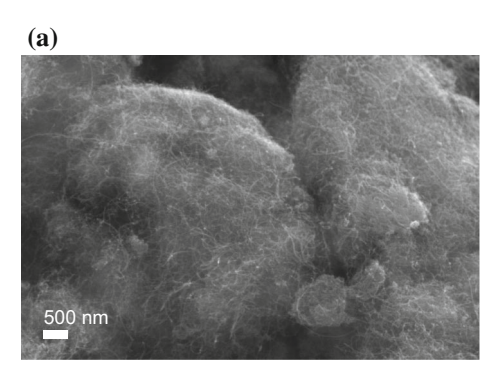


Table 2 Mixture design for the MWCNTs-reinforced geopolymers per 100 g of specimen

Sample name	Concentration (wt%)	MWCNTs (g)
KCT0.0	0.00	0.00
KCT0.3	0.29	0.10
KCT0.6	0.58	0.20
KCT1.5	1.47	0.50

KCT0.0 represents the plain geopolymer. KCT0.3, KCT0.6, and KCT1.5 represent geopolymers reinforced with 0.3, 0.6, and 1.5 wt% MWCNTs, respectively, per weight of metakaolin. For all mixture designs, 18.43 g of fumed silica, 19.87 g of potassium hydroxide, 27.61 g of water, and 34.08 g of metakaolin were used per 100 g of specimen

nanocomposites reinforced with 0.3, 0.6, and 1.5 wt% MWCNTs per mass of metakaolin were named KCT0.3, KCT0.6, and KCT1.5, respectively.

To synthesize 100 g of geopolymer nanocomposites, we used three steps as shown in Fig. 2. The first step was to pre-disperse MWCNTs in 27.61 g of deionized water using the ultrasonic energy provided by a VCX 750 ultrasonic horn (Sonics and Materials, Newtown, CT, USA). The dispersion energy was 2.8975 kJ per g of MWCNTs and per mL of deionized water. The dispersion energy was

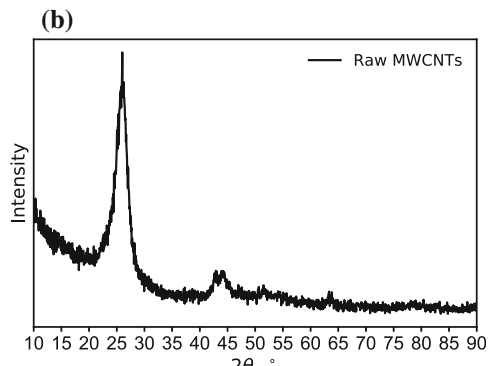
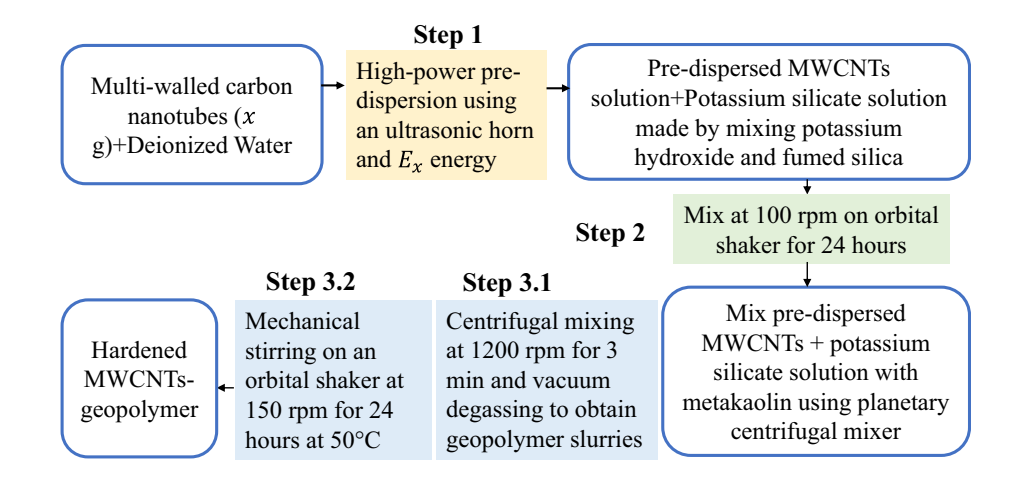




Figure 2 Manufacturing process for geopolymer nanocomposites.



proportional to the amount of MWCNTs. We used 8 kJ, 16 kJ, and 40 kJ of dispersion energy for KCT0.3, KCT0.6, and KCT1.5, respectively. To reduce the heat generated by the concentrated dispersion energy, an ice bath was implemented. The MWCNTs were further dispersed in the following two steps. The next step was to produce the potassium silicate solution. We mixed the well-dispersed MWCNTs suspension with 19.87 g of potassium hydroxide and 18.43 g of fumed silica until a uniform viscous solution was produced. The final solution continued to be mixed in a 3-mm orbital shaker at a rotational speed of 100 rpm at room temperature for 24 hours. Continuous stirring in the orbital shaker was used to prevent agglomeration and sedimentation of the MWCNTs within the potassium silicate solution.

The final step was to manufacture the geopolymer nanocomposites by mixing the potassium silicate solution with metakaolin using a planetary centrifugal mixer, THINKY ARE 310 (THINKY U.S.A., Laguna Hills, CA, USA). Mixing occurred in two stages. The first stage involved centrifugal mixing at 1200 rpm for 3 min. The second stage was vacuum degassing. We used proportional parameters for different concentration levels to account MWCNTs-induced increases in the viscosity of the MWCNTs-reinforced geopolymer slurries. selected vacuum degassing speeds and times were 1400 rpm for 3 min for KCT0.0 and KCT0.3, 1600 rpm for 5 min for KCT0.6, and 1800 rpm for 10 min for KCT1.5. The geopolymer slurries were then poured into 30-mm-diameter cylindrical molds and sealed with plastic wrap. The specimens were cured in an orbital shaker at a rotational speed of 150 rpm and under a temperature at 50 °C for 24 hours.

MWCNTs dispersion characterization and optical microscope characterization

To perform the dispersion characterization of the MWCNTs, for the solid state of MWCNTs reinforced geopolymers, we applied microscopic imaging using Amscope (Irvine, CA, USA) Infinity Plan Research Compound Microscope (40X–2500X) to evaluate the dispersion state. We took 100 images, 10 rows by 10 columns unrepeatable images for each sample using microscopic imaging. The image size was 0.65 mm in width and 0.49 mm in height. The image dataset of KCT0.0, KCT0.3, KCT0.6, KCT1.5 with scale bars and without scale bars were shared in the manuscript dataset. Afterwards, we used image processing software Image J and computer programming Python to make the image binary and obtain the image data. We plotted the grayscale histogram. Then, based on Pegel et al.'s image threshold algorithm [45] to find the binarization threshold. By applying the threshold, we characterized the MWCNTs dispersion. The data analysis technique and algorithm were put in Supplementary Material Information (SI). A.

Optical microscopy imaging was conducted using a Nikon high-resolution microscope. Afterward, the optical microscopy images were processed through digital image analysis to yield the meso-porosity. The image size was 1.04 mm in width and 0.83 mm in height. Images at different locations were used to calculate the average porosity. To validate the results obtained from the image analysis, we also measured the macro-porosity based on ASTM C20-00 [46] and Théréné *et al.* [47].



X-Ray diffraction and Fourier-transform infrared spectroscopy (FTIR)

X-ray powder diffraction was used to characterize the influence of MWCNTs on the chemistry of the geopolymer nanocomposites. Prior to testing, the samples were milled with ethanol using a McCrone mill (Retsch, Newtown, PA, USA) to generate a powder of uniform fineness, $\leq 44 \mu m$. X-ray powder diffraction tests were conducted at the J.B. Cohen Xray Diffraction Facility using a Smartlab Gen2 3kW Xray diffractometer (Rigaku Corporation, Tokyo, Japan) with an accessible energy of 40 keV, current of 30 mA, and Bragg angle of 2θ in the range of 10° to 90°. The step size was 0.05°. FTIR was performed using a Nicolet iS50 spectrometer (Thermo Fisher Scientific, Waltham, MA, USA) at the NUANCE Keck-II Facility. The powder specimens were prepared using the same method as for the X-ray powder diffraction analysis. In addition, KBr pellets were prepared by pressing a mixture of specimen powder and KBr (weight ratio of 1:100). The regular adsorption transmission mode was used with a frequency range of 4000 to 400 cm⁻¹, a resolution of 4 cm⁻¹, and an average of 64 scans. We applied statistical deconvolution on the FTIR results using the Python computer programming language [76].

Solid-state nuclear magnetic resonance

Solid-state nuclear magnetic resonance was applied to study the chemistry effects by MWCNTs. The 29 Si NMR spectrum was obtained at a 400 MHz Bruker Advance III HD system Hg400 (Bruker, Billerica, MA, USA). The Magic Angle Spinning (MAS) solid-state NMR was used to characterize the structure of silicon. Powdered specimens were packed into a 4-mm rotor. Spectrum was obtained with a spinning speed of 10 kHz with peak positions referenced to Si(SiMe3) of -9.84 ppm. Two thousand forty-eight transients were acquired using a single $\pi/4$ (10 μ s) relaxation delays.

Grinding and polishing

In order to perform microscopic testing, such as scratch tests and indentation tests, we implemented a rigorous specimen preparation procedure to yield a low surface roughness. The cured geopolymers were cold mounted into 35-mm-diameter cylindrical molds

using a low-viscosity epoxy resin. A high-precision, low-speed saw with a diamond blade was utilized to generate 5-mm thick cylindrical slices. The slices were mounted onto 35-mm-diameter aluminum disks. Digital photography images of the four types of geopolymer nanocomposites are shown in SI. B. Fig. 4. The mounted specimens were then ground and polished using a semi-automated grinder/polisher. Grinding was accomplished using silicon carbide abrasives of different grit sizes (400, 600, and 1200 grit, consecutively). Afterward, specimens were polished using synthetic long-napped rayon cloths with diamond suspensions of particle size 3 μ m, 1 μ m, and 0.05 μ m. In between each step, the specimens were rinsed for 2 min in an oil-based solution using an ultrasonic bath to avoid contamination. The polished surface was characterized by scanning electron microscope as shown in SI. B. Fig. 5. Afterward, the polished specimens were stored in a vacuum desiccator at room temperature.

Scratch testing

Scratch testing was utilized to evaluate the fracture behavior of geopolymer nanocomposites at the microscopic length-scale. Scratch testing consists of pulling a hard probe across the surface of the material under a prescribed linear vertical force. We used an Anton Paar microscopic scratch tester (Anton Paar, Ashland, VA, USA) equipped with a 200-µm Rockwell C diamond probe. For each type of geopolymer nanocomposite, we performed 11 scratch tests. Each test was characterized by a length of 3 mm, a scratch speed of 6 mm·min⁻¹, and a maximum vertical force of 5.5 N. The microscopic scratch was integrated with an optical microscope to get microscope images. The theory of scratch testing is described in details in SI. C. 1.

Micro-indentation testing

We implemented the grid indentation method to evaluate the mechanical behavior of the geopolymer nanocomposites. For each series of tests, an 11×11 array of indentation tests was conducted using a Berkovich indenter using Anton Paar nanohardness tester (Anton Paar, Ashland, VA, USA). The indenter contact area function was calibrated using fused silica prior to testing. Each indentation test was characterized by a maximum vertical force of 500 mN, a



loading/unloading rate of 1000 mN·min⁻¹, and a 10 second pause. The inter-indent spacing was 100 μ m. For each indent, the vertical force P and penetration depth h were recorded using high-resolution force and displacement sensors with a precision of 20 nN and 0.01 nm, respectively. For each indent, the indentation hardness H and indentation modulus M were calculated using Oliver and Pharr's method [51] as shown in Eq. (1):

$$H = \frac{P}{A_c}; M = \frac{\sqrt{\pi}}{2} \frac{S}{\sqrt{A_c}}; S = \frac{dP}{dh} \bigg|_{h=h_{max}}$$
 (1)

where S is the unloading slope. The contact area A_c was calculated from the maximum depth h_{max} using the calibrated contact area function for the indenter [51, 52]. More details of cluster analysis for indentation were put in SI. C. 2.

Rheology characterization

In order to characterize the rheology of the fresh geopolymer slurries, we used a modular compact rheometer equipped with a plate-plate system with a plate diameter of 24.98 mm. The measured distance was 0.25 mm, and the measuring temperature was 25.00 ± 0.05 °C. Flow curves in a shear rate ranging from 1 to $100 \, \mathrm{s}^{-1}$ were measured in 17 constant, logarithmically spaced steps with a time delay of 5 seconds between successive measurements. The modified Bingham model (MBM) was implemented to fit the shear stress and shear rate curves as shown in Eq. (2) due to the non-Newtonian nature of the fresh geopolymer nanocomposites:

$$\tau = \tau_0 + \eta_p \cdot \gamma + c\gamma^2 \tag{2}$$

where τ is the shear stress, γ is the shear rate, and c is a constant. Yield shear stress τ_0 and plastic viscosity η_p are the rheology characteristics. The rheology parameters–yield shear stress τ_0 and plastic viscosity η_p —were determined through nonlinear fitting of Eq. (2) [30] using the Python computer programming language.

Results

Dispersion characterization

Figure 3 presents the presence of dispersed MWCNTs. More details including the MWCNTs size

histogram distribution were put in SI. D. For KCT0.3, the MWCNTs size was less than 8 μ m² with an average of 5.423 μ m². For KCT0.6, it was less than 10 μ m² with an average of 6.631 μ m², while for KCT1.5, all sizes were less than 13 μ m² with an average of 8.899 μ m². With the increase in concentration levels, the average size becomes larger, which means that the dispersion was more challenging. The results showed that all MWCNTs were well dispersed.

Microstructure characterization

To characterize the microstructure of MWCNTs reinforced geopolymers, we employed high-resolution scanning electron microscope. Figures 4 and 5 present the cross section of geopolymer reinforced with MWCNTs. We can observe MWCNTs for all three types of geopolymer nanocomposites. Figure 5 presents the presence of MWCNTs in pore structure. Figure 4 displays MWCNTs growing in geopolymer matrix. Figure 4 shows that MWCNTs was very well dispersed in geopolymer matrix. More SEM images were put in SI. H. From the microstructure, MWCNTs were well dispersed in the geopolymer matrix, and some part of MWCNTs grow inside the geopolymer matrix and connect as bridges for fracture surfaces.

With the addition of MWCNTs, the size of the pores decreased. To quantify the change in microporosity, we applied digital image analysis. More details of image analysis approach can be found in SI. A. The computed average microporosity values were 8.698, 4.576, 5.664, and 7.072% for KCT0.0, KCT0.3, KCT0.6, and KCT1.5, respectively. Overall, we noted a decrease in microporosity in MWCNTs-reinforced geopolymers compared to the plain geopolymer. KCT0.3 showed a 47.39% decreases in the microporosity. To validate the results obtained from the image analysis, we also measured the macro-porosity based on ASTM C20-00 [46] and Théréné et al. [47]. We observed the same trend for the macro-porosity, with values of 11.98, 11.60, 9.83, and 10.72% for KCT0.0, KCT0.3, KCT0.6, and KCT1.5, respectively. More details are shown in SI. A. 1.3. MWCNTs decreased the macroporosity. However, 0.6 wt% was the optimum concentration level. MWCNTs addition decreased both the microporosity and macroporosity. However, for the other two MWCNTs-reinforced geopolymers, we noted a slight increase in



Figure 3 Microscopic images of a KCT0.0, b KCT0.3, c KCT0.6, and d KCT1.5.

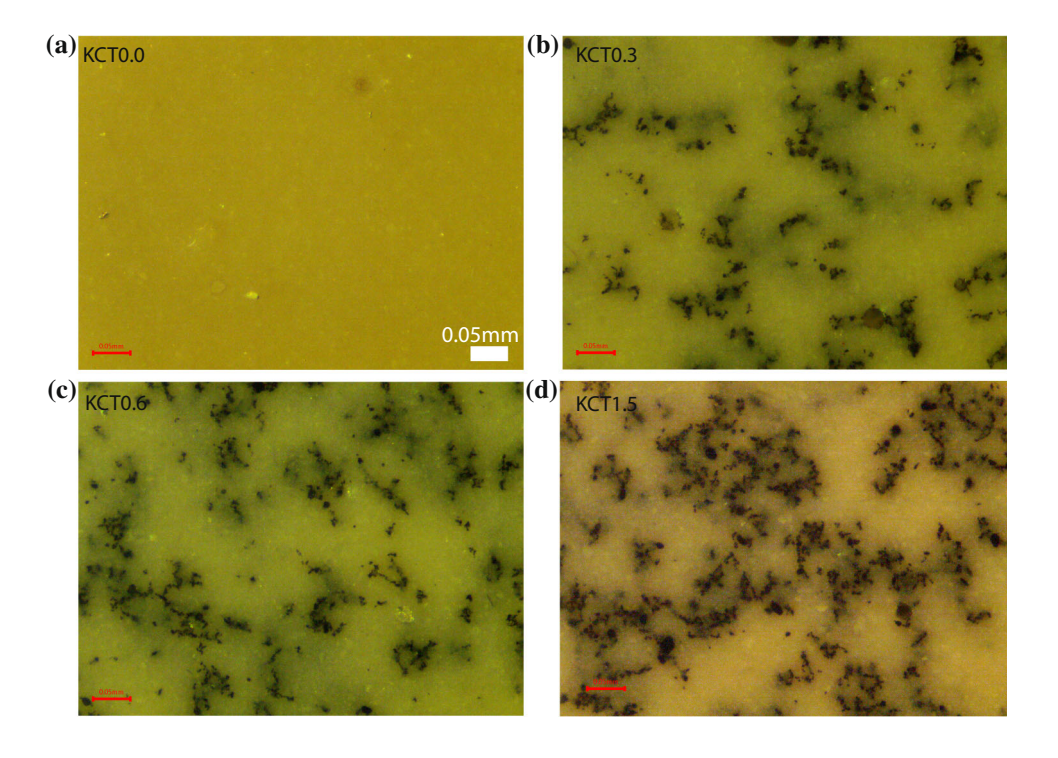
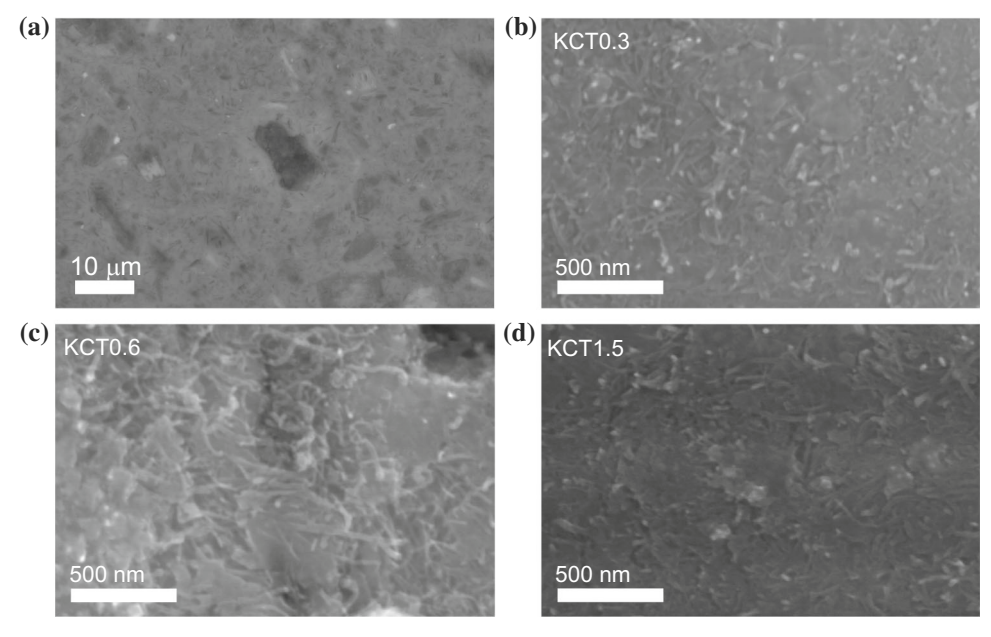


Figure 4 SEM: a Plain geopolymer, KCT0.0; b Geopolymer reinforced with 0.3 wt% MWCNTs, KCT0.3; c Geopolymer reinforced with 0.6 wt% MWCNTs, KCT0.6; d Geopolymer reinforced with 1.5 wt% MWCNTs, KCT1.5 at 100, 000x.



microporosity as the fraction of MWCNTs reinforcement increased. Overall, the porosity decreased with the addition of MWCNTs compared to the plain geopolymer.

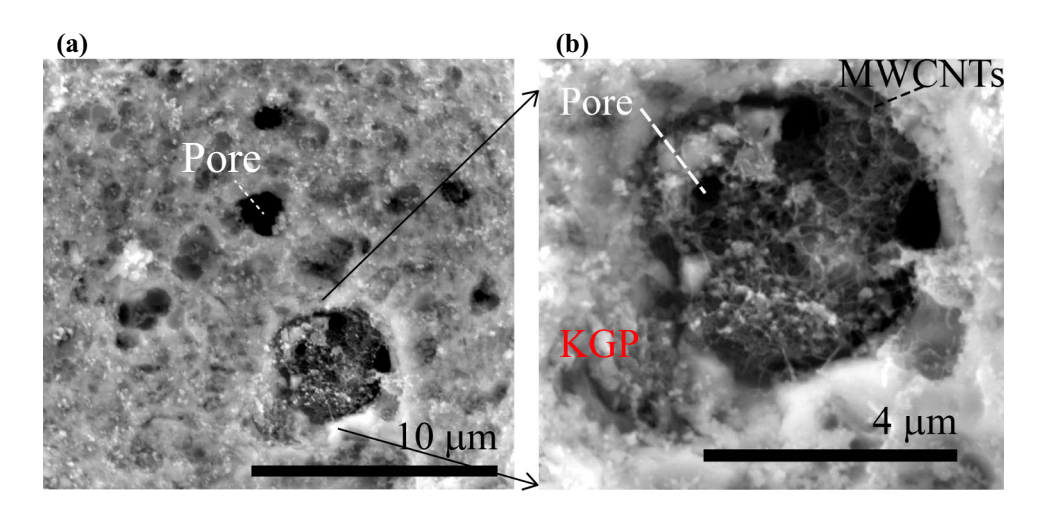
X-Ray powder diffraction and FTIR

To understand the chemical influence of MWCNTs on the chemistry of the geopolymer nanocomposites in their hardened state, we applied X-ray powder

diffraction (XRD) and FTIR. Figure 6 displays the X-ray diffractograms for the geopolymer nanocomposites. For KCT0.0, the X-ray diffraction was amorphous with a broad peak located around $2\theta=28^{\circ}$. The sharp peak located around $2\theta=25^{\circ}$ refers to the titanium dioxide present in the raw metakaolin material. The results show that MWCNTs preserved the amorphous structure of the geopolymer nanocomposites.



Figure 5 a Microstructure of the geopolymer matrix and pore phase of KCT1.5; b MWCNTs connect the geopolymer pores and grow with the geopolymer matrix to fill the pore (KCT1.5).



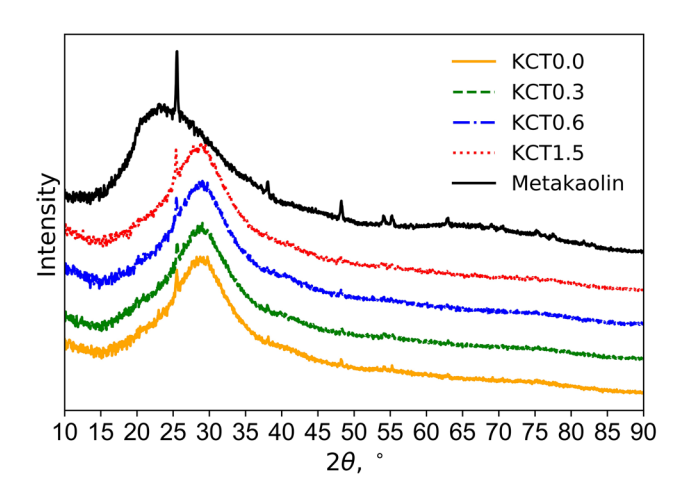


Figure 6 X-Ray powder diffraction results for KCT0.0 (*green*), KCT0.3 (*blue*), KCT0.6 (*red*), KCT1.5 (*black*), and metakaolin (*orange*). Data are displayed as stacked.

The FTIR spectra are shown in Fig. 7. We focused on the wavenumber range of 400-1200 cm⁻¹. We observed three main peaks. The first peak was around 840 cm⁻¹ and represented the Si-OH bending vibration. The second peak was around 1008 cm⁻¹ and represented the asymmetrical vibration of Si(Al)-O [65]. Finally, the third peak was around 1080-1100 cm⁻¹ and represented the symmetrical vibration of Si-O [66]. We observed a decrease in the wave number characteristic of the bending vibration of Si-OH. This decrease points to an increase in the mass of the Si-OH bonds. Thus, it can be concluded that MWCNTs promote the formation of Si-OH bonds. In return, there was a decrease in the wave number characteristic of symmetrical vibration in the Si-O bonds, pointing to a reduction in Si-O bonds. Finally, the wave number for the asymmetrical vibration for Si(Al)-O remained the same for KCT0.3 and KCT0.6 and decreased for KCT1.5. A prior study related the frequency of the Si(Al)-O asymmetrical vibration

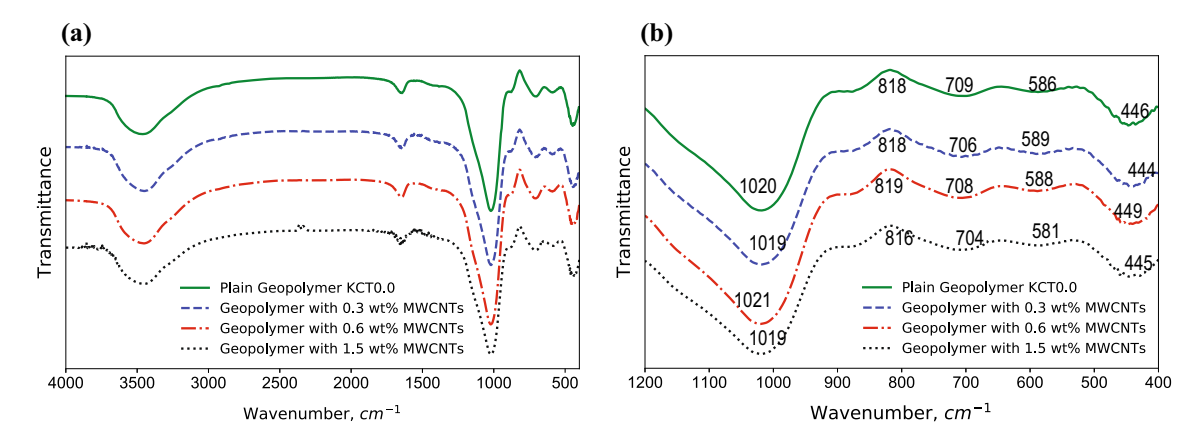


Figure 7 FTIR results: a 450–4000 cm⁻¹ full spectrum; b 400–1200 cm⁻¹ with peaks.

band to the Si/Al ratio [67]. However, more analysis needs to be done to characterize the change is Si-O bonds.

NMR results

To characterize the Si-O bonds, we implemented solid state ²⁹Si NMR. The solid-state NMR results are shown in Fig. 8 and Table 3. The solid NMR results display a single broad resonance. For plain geopolymer KCT0.0, the peak occurs at -92.3604 ppm with 18141.2 intensity. Our plain geopolymer Si/Al = 2. The plain metakaolin NMR results agree with previous studies on metakaolin geopolymers with Si/Al = 1.9-2.15 [76-82]. More details of NMR fraction analysis are shown in SI. E. For geopolymer reinforced with 0.3 and 0.6 wt% MWCNTs, the peak occurs at the same position -91.7456 ppm, with 18584.4, 18763.5 intensity, respectively. For 1.5 wt% MWCNTs, the peak shifted back to -92.9753 ppm with the intensity of 18243.2. This result helps us to understand the chemical structure effects by different concentration levels of MWCNTs in geopolymer system.

Fracture toughness of geopolymer nanocomposites

Scratch testing was conducted to understand the influence of MWCNTs reinforcement on the fracture performance. The results of the scratch test are shown in Fig. 9. The quantity $F_T/\sqrt{2pA}$ was plotted along the scratch length X, where F_T is the horizontal force,

Table 3 Results of ²⁹Si Solid-State NMR MAS

Name	KCT0.0	KCT0.3	KCT0.6	KCT1.5	Metakaolin
Peak, ppm	-92.36	-91.74	-91.74	-92.97	-103.428
Intensity	18141	18584	18763	18243	13502

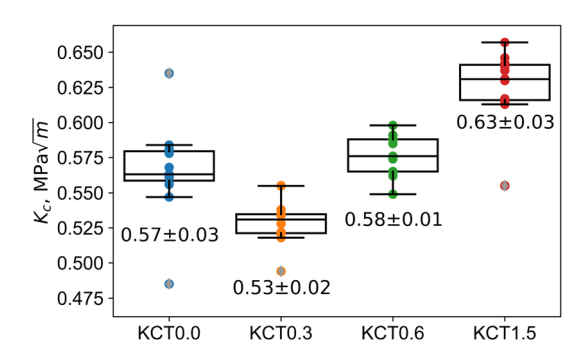


Figure 9 Scratch results for KCT0.0, KCT0.3, KCT0.6, and KCT1.5.

and 2pA is the scratch probe shape function. At the beginning of the scratch, penetration depths were relatively low, which resulted in extreme variation in the results of $F_T/\sqrt{2pA}$. At this stage, the fracture mechanisms combined plasticity and elasticity. With the development of the scratch, $F_T/\sqrt{2pA}$ reached a convergence regime. The convergence of $F_T/\sqrt{2pA}$ indicates that the fracture mechanism developed from ductile to brittle. The linear elastic fracture mechanics dominated in this area. Plots of the converging fracture toughness analysis of each sample can be found in SI. F.

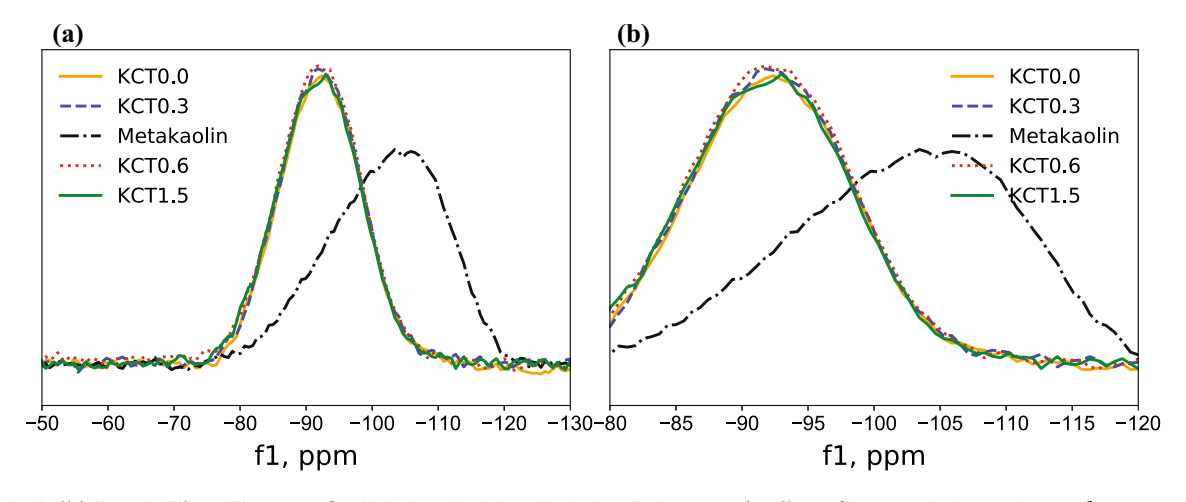


Figure 8 Solid-State 29Si MAS NMR of KCT0.0, KCT0.3, KCT0.6, KCT1.5, Metakaolin: **a** f1 range -150 to -50 ppm; **b** narrower range −120 to −80 ppm.



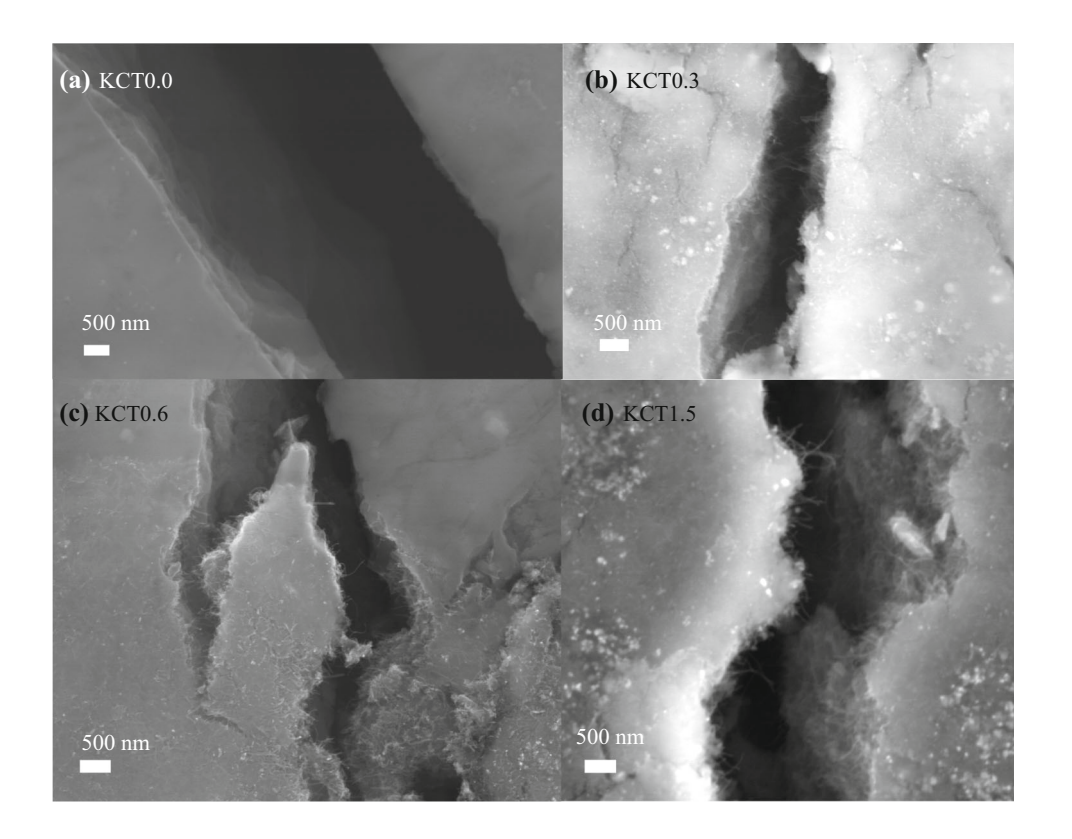
The fracture toughness value of the plain geopolymer was 0.57 ± 0.03 MPa \sqrt{m} , which agrees with the fracture toughness of the plain metakaolin geopolymer measured at the macroscopic scale using three-point bending tests [42]. Therefore, the model to assess the fracture toughness at the microscopic scale is valid. High fractions of MWCNTs improved the fracture toughness of the metakaolin-based potassium geopolymers. The fracture toughness values were 0.53 ± 0.02 , 0.58 ± 0.01 , and 0.63 ± 0.03 MPa.m^{0.5} for KCT0.3, KCT0.6, and KCT1.5, respectively. We observed a decrease in fracture toughness with the addition of 0.3 MWCNTs. There was a 1.75% increase in fracture toughness with the addition of 0.6 wt% MWCNTs. Finally, there was a huge increase (10.52%) in fracture toughness compared to the plain geopolymer with the addition of 1.5 wt% MWCNTs.

Scanning electron microscope images (Fig. 10a) showed that the fracture surfaces of pure geopolymer, while Fig. 10b, c, d shows that MWCNTs acted as bridges between fracture surfaces and connected the geopolymer matrix. Figure 10b, c, d shows that the MWCNTs pull-out effects, where MWCNTs worked as fiber reinforcement.

Figure 10 Fracture surface demonstrating that MWCNTs act as bridges to connect the geopolymer matrix relationships: a Pure geopolymer KCT0.0; b Geopolymer reinforced with 0.3 MWCNTs, KCT0.3; c Geopolymer reinforced with 0.6 MWCNTs, KCT0.6; d Geopolymer reinforced with 1.5 wt% MWCNTs, KCT1.5.

Grid indentation and cluster analysis results

Grid indentation was implemented to characterize the underlying mechanical phases at the microscopic length scale, based on the distribution of the indentation modulus M, indentation hardness H, and local microporosity ϕ . Figure 11 displays the histograms of the indentation modulus. Histograms of the indentation hardness can be found in SI. G. Indentation Hardness. The presence of MWCNTs affected the frequency of the indentation modulus. We also observed a broadening of the peak of the indentation modulus, which points to an increase in the heterogeneity levels as the fraction of MWCNTs increased. The measured average indentation modulus was 7.76 \pm 0.23, 7.83 \pm 0.31, 8.01 \pm 0.44, and 7.48 \pm 0.49 GPa for the plain geopolymer, KCT0.3, KCT0.6, and KCT1.5, respectively. Thus, the average indentation modulus increased by 0.9 and 3.2% with the addition of 0.3 and 0.6 wt% MWCNTs, respectively. However, incorporating 1.5 wt% MWCNTs decreased the indentation modulus by 3.6%. Similarly, the measured average indentation hardness was 388.27 \pm 16.93, 414.41 \pm 23.60, 431.33 \pm 37.67, and 392.31 \pm 41.20 MPa for the plain geopolymer, KCT0.3, KCT0.6, and KCT1.5, respectively. The indentation hardness





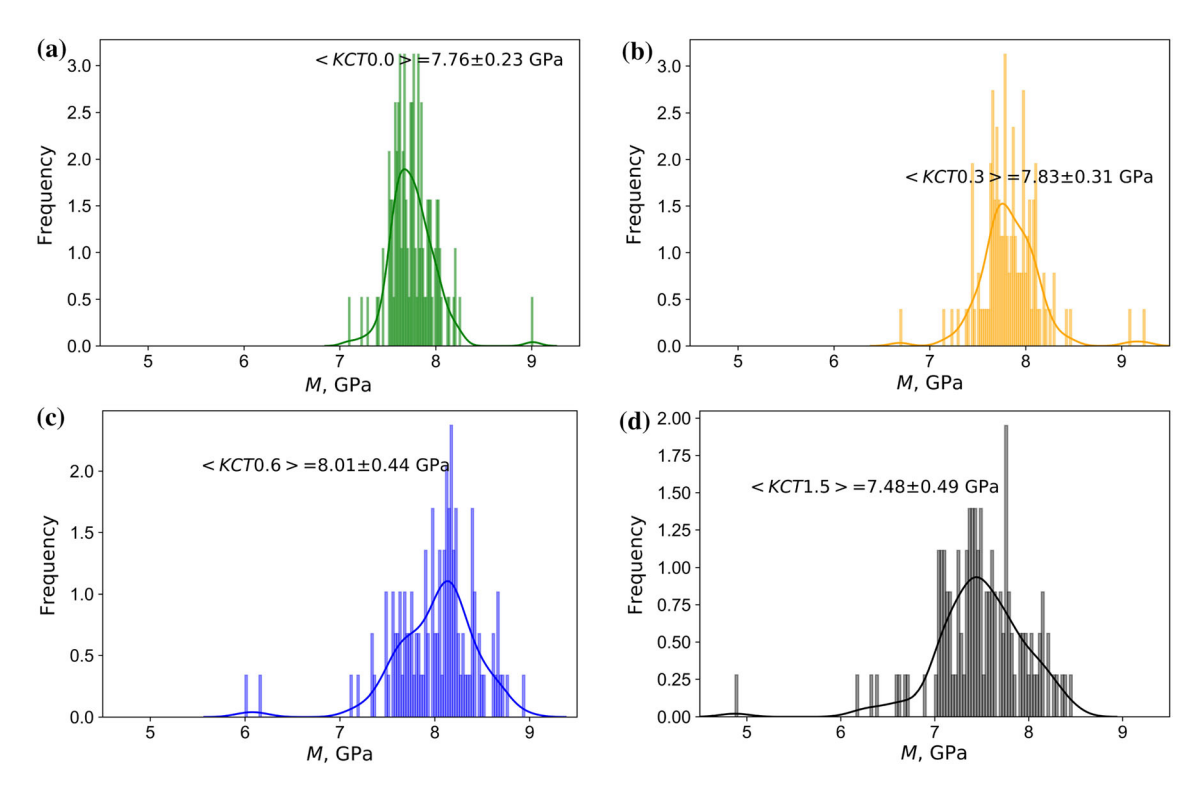


Figure 11 Indentation modulus M histogram: a KCT0.0 (green), b KCT0.3 (orange), c KCT0.6 (blue), and d KCT1.5 (black).

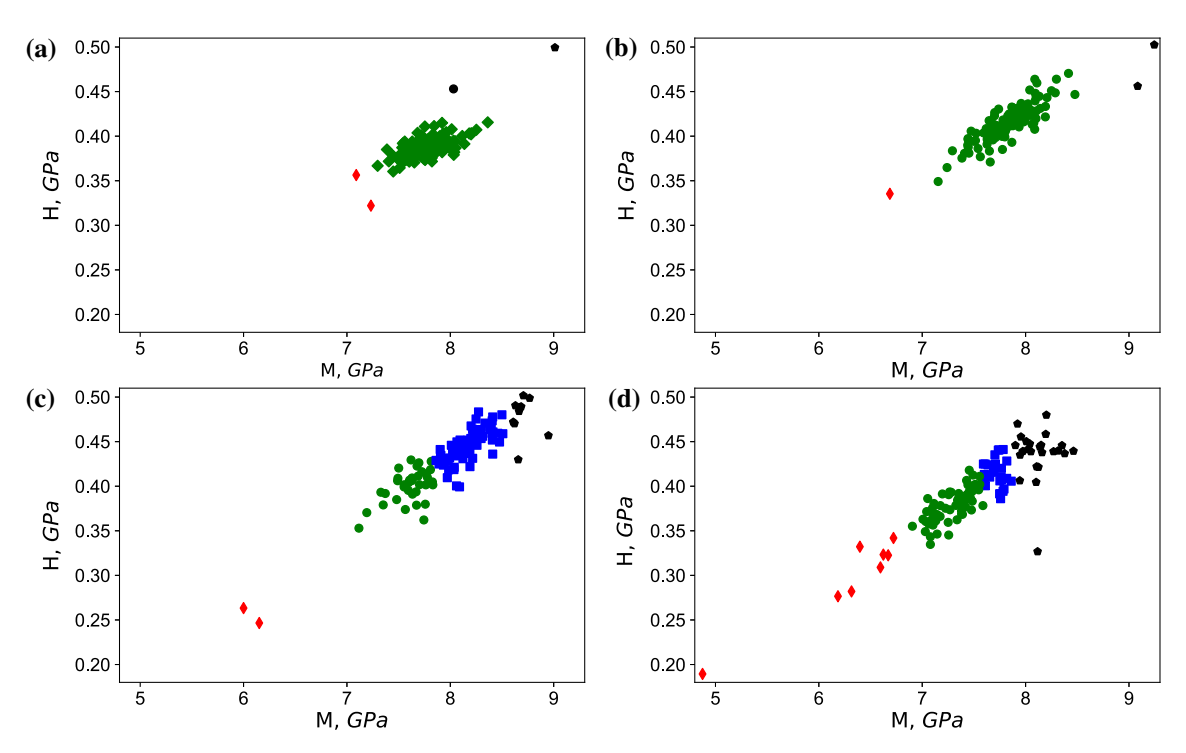


Figure 12 Cluster analysis of the indentation hardness H (GPa) and indentation modulus M (GPa): **a** KCT0.0, **b** KCT0.3, **c** KCT0.6, and **d** KCT1.5. *Red circles* represent the geopolymer

with porous phase, *green circles* represent the main geopolymer phase, *blue squares* represents geopolymer phase, and *black circles* represent a much stronger geopolymer phase.



results were put in SI. G. Thus, the addition of MWCNTs increased the indentation hardness by 6.7, 11.1, and 1.04% for 0.3, 0.6, and 1.5 wt% MWCNTs, respectively.

We implemented cluster analysis using the Gaussian mixture method to quantify the phase transformation and shift. Figure 12 displays the results of the cluster analysis. The detailed characteristics for all phases in all specimens are given in Table 4.

The main phase of the plain geopolymer had an indentation modulus of 7.759 GPa, an indentation hardness of 0.388 GPa, and a porosity of 8.7%. For KCT0.3, the main phase characteristics increased to 7.822 GPa for the indentation modulus and 0.414 GPa for the indentation hardness; meanwhile, the porosity decreased to 5.6%. For KCT0.6, the reinforcement effects prevailed, with the main phase characteristics increasing to 8.171 GPa for the indentation modulus and 0.445 GPa for the indentation hardness, and the porosity decreasing to 5.1%. For KCT0.6, there was a weaker phase, with an indentation modulus of 7.620 GPa, indentation hardness of 0.401 GPa, and porosity of 7.4%. However, for KCT1.5, a bimodal distribution with two dominating phases was observed. In the

weaker phase, an indentation modulus of 7.407 GPa, indentation hardness of 0.387 GPa, and porosity of 7.5% were observed. In the stronger phase, an indentation modulus of 8.114 GPa, indentation hardness of 0.436 GPa, and porosity of 0.45% were observed.

Here, we recall the NMR results (see Fig. 8) and indentation statistical results (see Table 4), in which KCT0.3, KCT0.6, and KCT1.5 showed an increase in atomic structural changes (Q⁴(Al3)), due to the geopolymerization. However, for KCT1.5, it showed a smaller increase compared to KCT0.3 and KCT0.6. The indentation results agree with the NMR results and show that KCT0.6 exhibited the highest values for the indentation modulus and hardness. Overall, our indentation results show that the addition of MWCNTs promoted the growth of a stronger geopolymer phase.

Rheology test results

We employed rheology tests to investigate the behavior of the geopolymer nanocomposites under a fresh state. Figure 13a shows the evolution of the

Table 4 Cluster analysis volume fraction results

Sample name	Phase	Volume fraction	μ^M GPa	s^M GPa	μ^H GPa	s^M GPa	μ^ϕ	s^ϕ
KCT0.0	Porous phase	0.015	7.166	0.003	0.338	0.002	0.114	0.004
	Geopolymer	0.944	7.759	0.038	0.388	0.000	0.087	0.000
	Geopolymer	0.008	7.763	0.002	0.388	0.003	0.087	0.007
	Stronger phase	0.016	8.031	0.001	0.453	0.003	0.076	0.005
	Stronger phase	0.016	9.011	0.002	0.499	0.003	0.037	0.005
KCT0.3	Porous phase	0.012	6.688	0.002	0.335	0.003	0.108	0.005
	Geopolymer	0.967	7.822	0.056	0.414	0.001	0.056	0.000
	Geopolymer	0.008	7.834	0.002	0.415	0.003	0.055	0.007
	Geopolymer	0.000	7.834	0.002	0.415	0.003	0.055	0.007
	Stronger phase	0.012	9.164	0.004	0.479	0.002	0.003	0.004
KCT0.6	Porous phase	0.022	6.077	0.004	0.255	0.002	0.150	0.004
	Geopolymer	0.303	7.620	0.032	0.401	0.001	0.074	0.001
	Geopolymer	0.000	8.012	0.002	0.431	0.003	0.058	0.007
	Stronger	0.607	8.171	0.029	0.445	0.000	0.051	0.000
	Stronger phase	0.067	8.700	0.008	0.481	0.001	0.030	0.002
KCT1.5	Porous phase	0.073	6.312	0.237	0.298	0.002	0.130	0.003
	Geopolymer	0.183	7.097	0.005	0.363	0.001	0.090	0.001
	Geopolymer	0.320	7.407	0.009	0.387	0.000	0.075	0.000
	Geopolymer	0.227	7.713	0.007	0.414	0.001	0.062	0.001
	Stronger phase	0.198	8.114	0.022	0.436	0.001	0.045	0.001

 μ^M : average indentation modulus; μ^H : average indention hardness; μ^{ϕ} : average porosity; s^M : standard deviation of indentation modulus; s^H : standard deviation of indentation hardness; s^{ϕ} : standard derivation of porosity



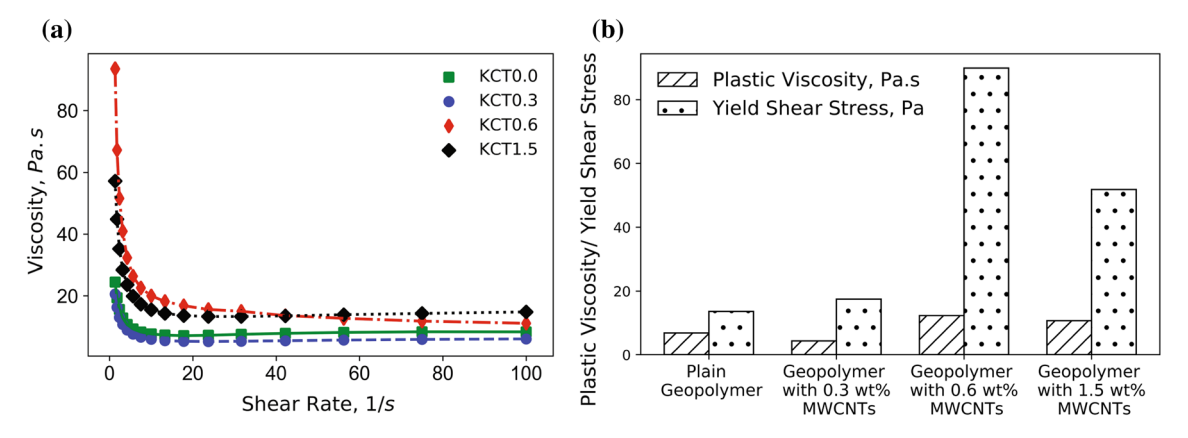


Figure 13 a Viscosity η —shear rate relationships; b Bar plot of plastic viscosity η_v and yield shear stress τ_0 .

viscosity for different shear rates. Figure 13b shows the bar plot of plastic viscosity and yield stress after MBM fitting. The shear stress-shear rates curves and the MBM fitting curves are shown in SI. We observed a shear-thickening non-Newtonian behavior. The results demonstrated that the addition of 0.3 wt% MWCNTs decreased the plastic viscosity compared to the plain geopolymer. However, for KCT0.6 and KCT1.5, we observe a higher plastic viscosity and shear stress compared to the plain geopolymer. When the shear rate was less than 40 s⁻¹, KCT0.6 had the highest plastic viscosity. However, when the shear rate increased, KCT1.5 had the highest plastic viscosity. The plastic viscosity and yield shear stress values obtained from the MBM are shown in Table 5. There was an increasing trend of yield shear stress with the addition of MWCNTs (Fig. 13b). For KCT0.6 and KCT1.5, we noted 79.79 and 56.37% increases in plastic viscosity, respectively. Similarly, the yield shear stress increased by 28.29, 560.32, and 280.96% for KCT0.3, KCT0.6, and KCT1.5, respectively.

Table 5 Rheology results

Specimen	$ \eta_p $ (Pa·s)	$ au_0,$ Pa	c	R^2
KCT0.0	6.83	13.61	0.015	0.999956
KCT0.3	4.32	17.46	0.016	0.999957
KCT0.6	12.28	89.87	-0.021	0.999975
KCT1.5	10.68	51.85	0.037	0.999987

 η_p : plastic viscosity; τ_0 : yield shear stress; R^2 : coefficient of determination

Discussion

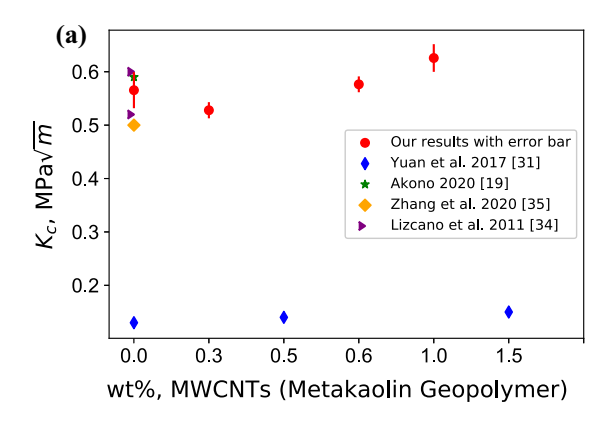
Dispersion state and microstructure

Based on the image analysis, we found out that the MWCNTs accumulated area was in the range of 2–13 μ m², which is quite low compared to previous literature on construction materials with MWCNTs. To our knowledge, there was few reported results on dispersion state characterization of geopolymer with MWCNTs using microscopic image. Thus, we compared our results to a similar functionality, classic construction material cement results published in peer-reviewed top journals. Zou *et al.* obtained 179.446 μ m² for the average area of CNTs in cement system [74]. Zhan *et al.* obtained 1367.25 μ m² and 52.48 μ m² in CNTs in cement system [75]. Comparison with previous literature results, our method to disperse MWCNTs is valid and efficient.

Combining the results from the chemical characterization with the indentation results, MWCNTs stiffen the metakaolin-based geopolymer matrices. For mass fractions of 0.3 and 0.6 wt% MWCNTs, the average indentation modulus increased as the mass fraction of MWCNTs increased. The sharp decline in the indentation modulus for 1.5 wt% MWCNTs can be explained by the increase in microporosity.

Porosity determines the strength of geopolymers [57]. Compared to the plain geopolymer, the porosity was reduced by 47.3, 34.8, and 18.7% with the addition of 0.3, 0.6, and 1.5 wt% MWCNTs, respectively. The computed average microporosity value was 8.698, 4.576, 5.664, and 7.072% for KCT0.0, KCT0.3, KCT0.6, and KCT1.5, respectively. Compared to a study on potassium geopolymer foams with CNTs





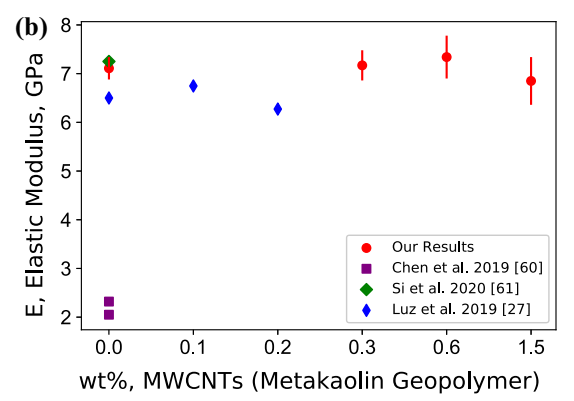


Figure 14 a Fracture Toughness with reference; b Elastic Modulus with reference.

[73], the porosity in our study was much smaller and they also noticed the reduction with the reinforcement of MWCNTs. Yan et al. [73] used foamed geopolymers instead of normal geopolymers, and we used a different dispersion procedure. Moreover, we noted an increase in microporosity as the fraction of MWCNTs reinforcement increased. Using Hashin-Shtrikman bounds, the Young's modulus for KCT0.0, KCT0.3, and KCT0.6 are in the predictive range, which indicates that the porosity fraction of the geopolymer is quite low. Recalling the rheology test results, the plastic viscosity increased as the fraction of MWCNTs increases, which may explain the observed increase in microporosity for the MWCNTsreinforced geopolymers. Thus, we observed two competitive trends. On the one hand, MWCNTs led to a reduction in pore size and pore fraction; on the other hand, the increase in plastic viscosity of the MWCNTs-reinforced geopolymer slurries promoted the development of microscopic air voids. MWCNTs act as fillers to connect the geopolymer pores and grow with the geopolymer matrix to fill the pore.

Effects of MWCNTs on chemical properties

The X-ray diffraction results showed that MWCNTs preserved the amorphous structure of metakaolin-based potassium geopolymers. The statistical FTIR results showed that MWCNTs affected chemical bonds; specifically, we observed an increase in Si-OH bonds and a reduction in Si-O bonds. Thus, MWCNTs promote the hydroxylation of Si atoms in the geopolymer. This inner strengthening is corroborated by the densification in microstructure. Moreover, this inner strengthening effect was also

observed in the statistical deconvolution results as the mechanical properties of the dominant phase increased.

Davidovits studied that the broad peak was comprised of all five possible silicon Q^4 (mAl) species including Q^4 (4Al), Q^4 (3Al), Q^4 (2Al), Q^4 (1Al), and Q^4 (0Al), which are resonating at approximately -84, -89, -93, -99, and -108 ppm, respectively [1, 78, 82]. Therefore, the deconvolution is based on the five possible silicon Q^4 (mAl). From our results, we have more Q^4 (2Al) since our Si/Al ratio is 2. With the addition of 0.3 and 0.6 wt% MWCNTs, it seems that there was a little more fraction of Q^4 (3Al). However, for 1.5 wt% MWCNTs, we have more Q^4 (3Al). This may be due to the cluster effects by high concentration MWCNTs.

Enhancement in fracture resistance

Our microscopic fracture tests indicated a positive correlation between the fracture toughness and the mass fraction of MWCNTs for metakaolin-based geopolymers. Rovnanik et al. [40] found that fly ash geopolymer mortars with a low concentration of MWCNTs (0.05 and 0.1 with respect to fly ash) decreased the fracture toughness by 9 and 13%, respectively. Rovnanik et al. found that 0.15 and 0.2% MWCNTs can increase the fracture toughness by 7 and 10%, respectively. Even though they used mortar and a different type of aluminosilicate source (fly ash), our results showed a similar trend. For Rovnanik et al. [40], their fracture toughness of fly ash based geopolymer mortars was in the range of 0.175–0.300 MPa· \sqrt{m} , which was smaller than the plain



metakaolin geopolymer reported in another study [42]. Yuan et al. [33] found that high concentration levels of MWCNTs enhanced the fracture behavior of metakaolin-based geopolymers using a classical macroscopic method. However, their fracture toughness values were quite low, ranging from 0.12 to 0.18 MPa· \sqrt{m} (fracture toughness of the plain geopolymer was around 0.12 MPa· \sqrt{m} in their study). This plain geopolymer value disagrees with that of other studies, which showed values of 0.5 MPa· \sqrt{m} by Zhang et al. [42] and 0.52–0.60 MPa· \sqrt{m} by Lizcano et al. [41] as shown in Fig. 14.

Our tested fracture toughness was in the range of 0.475-0.66 MPa $\cdot\sqrt{m}$. As mentioned previously, the fracture toughness value of our plain geopolymer using microscopic scratch testing was 0.57 ± 0.03 MPa $\cdot \sqrt{m}$, which agrees with the fracture toughness of previous study (around 0.5 MPa \sqrt{m} for the plain metakaolin geopolymer measured at the macroscopic scale using three-point bending tests reported in a recent study by Zhang et al. [42] and a previous study by Lizcano et al. [41]. We observed that the addition of 0.3 wt% MWCNTs slightly decreased the fracture toughness while 0.6 and 1.5 wt% MWCNTs increased the fracture toughness by 1.75 and 10.52%, respectively. Moreover, we observed a small decrease in fracture toughness for 0.3 MWCNTs and an increase for 0.6 and 1.5 wt% MWCNTs.

We observed that for plain geopolymer, there were no pull-out effects or bridging effects. However, for the geopolymer reinforced with 0.3, 0.6, 1.5 wt% MWCNTs, we can observe those effects by MWCNTs, which lead to the increase in fracture toughness. For plain geopolymer, we obtained a fracture toughness value from 0.485 to 0.635 MPa \sqrt{m} while the fracture toughness of geopolymer reinforced with 0.3 wt% MWCNTs ranges from 0.494 to $0.595 \text{ MPa}\sqrt{m}$. If we focus on the lowest value of the geopolymers, MWCNTs increased the fracture toughness. However, considering the highest values and average values, 0.3 wt% MWCNTs decreased the fracture toughness. This decrease in the fracture toughness can be explained by an increase in capillary porosity or pre-existing cracks. This decline can also be explained by a lower level of concentration of MWCNTs which would inhibit their crack bridging potential. Previous literature also observed a decline in fracture toughness. The decline in fracture toughness was related to the increase in strength and hardness at the same time. MWCNTs act as bridges and pull-out "fibers" to enhance the fracture toughness in the geopolymer matrix.

Indentation result

In the meanwhile, indentation results and indentation analysis using Gaussian mixture method to quantify the phase transformation and shift showed that the addition of MWCNTs promoted the growth of a stronger geopolymer phase. The results of our elastic modulus test via indentation (using 10 mN of force) of the plain metakaolin agrees with a previous study by Si et al. [72] as shown in Fig. 14b. Moreover, Chen et al. [71] used nanoindentation to test the creep behavior of a metakaolin sodium geopolymer using 50 mN of indentation force and obtained a lower value for the elastic modulus. The scanning electron microscope image shown in Fig. 13 demonstrates that MWCNTs connect the geopolymer matrix in the pore phase. Our indentation results agree with the microstructure results by SEM. For KCT0.3, we observed a 0.9% increase in the indentation modulus, and 6.73% increase in the indentation hardness. The addition of 0.6 wt% MWCNTs increased the indentation modulus and hardness by 3.2 and 11.1%, respectively. However, 1.5 wt% MWCNTs decreased the indentation modulus by 3.6% and increased the indentation hardness by 1.04%. For 0.6 and 1.5 wt% MWCNTs, the results showed a bimodal distribution with two dominant phases while the plain geopolymer and KCT0.3 only had one dominant phase. The analysis showed that MWCNTs promote a stronger phase. The addition of 0.6 and 1.5 wt% MWCNTs promoted another main phase, with the indentation modulus increasing from 7.759 GPa (plain geopolymer) to 8.171 GPa (5.30% increase) and 8.114 GPa (4.57% increase), respectively. At the same time, 0.6 and 1.5 wt% MWCNTs developed another main phase, with the indentation hardness increasing from 0.414 GPa (plain geopolymer) to 0.445 GPa (7.49% increase) and 0.436 GPa (5.31% increase), respectively. The elastic modulus obtained by indentation in our study agrees with elastic modulus results obtained in other studies [29, 71, 72] (Fig. 14b). Moreover, da Luz et al. [29] showed that a decrease in the elastic modulus with the addition of 0.1 MWCNTs, our results showed an increase in the elastic modulus with the addition of 0.3 and 0.6 wt% MWCNTs, indicating a suitable dispersion method.



Furthermore, we conducted an extended investigation of geopolymers reinforced with different levels of MWCNTs. Our quantitative results showed that MWCNTs promote geopolymerization.

Our study showed that the addition of MWCNTs promoted the geopolymer to grow another stronger phase and promoted geopolymerization in the metakaolin-based potassium geopolymers. Moreover, the indentation results agree with the NMR results and show that KCT0.6 exhibited the highest values for the indentation modulus and hardness. Furthermore, MWCNTs influence the chemistry and MWCNTs grow in and connect the pores in the geopolymer matrix. This microstructure enhancement effect was related to the increase in both indentation modulus and indentation hardness. Using SEM and indentation phase distribution results, we conclude that MWCNTs help the geopolymer to grow a stronger phase.

Rheology of the fresh state

In terms of rheology, two of the most important factors in 3-D printing of geopolymers are the plastic viscosity and the yield shear stress [68, 69]. Our plain geopolymer KCT0.0 had a yield stress of 13.61 Pa. This value agrees with that on a previous study on construction geopolymers [30]. Moreover, our measured yield shear stress for the plain geopolymer KCT0.0 also agrees with the yield stress range (11.5-13.6 Pa) reported by da Luz et al. [29] using mini-slump consistency tests. However, we provide additional insights on the effect of MWCNTs on the rheology. Da Luz et al. [29] reported that low fractions of MWCNTs would have little effect on the rheological properties of geopolymers; however, they only considered 0.1 and 0.2 of MWCNTs per weight of metakaolin. For the higher fractions of MWCNTs (> 0.3 wt%), we found that MWCNTs had a contradictory effect on the rheological properties. For KCT0.6 and KCT1.5, the plastic viscosity increased by 79.8 and 56.37%, respectively. Finally, the yield shear stress value increased by 28.29, 560.32, and 280.96% for KCT0.3, KCT0.6, and KCT1.5, respectively.

The plastic viscosity for geopolymer nanocomposites was in the same viscosity range as geopolymer mortars used for 3-D printing [70]. The increase in both the yield shear stress and plastic viscosity makes MWCNTs-reinforced geopolymer inks an attractive option for 3-D printing applications. In addition, the

MWCNTs fraction influenced the rheological properties. As a result, in future applications, the yield stress and plastic viscosity can be tailored by adjusting the fraction of reinforcing nanomaterials like MWCNTs so as to simultaneously optimize the rheological behavior in the fresh state and the mechanical properties in the hardened state.

Conclusions

We studied four types of metakaolin based potassium geopolymer nanocomposites: a plain geopolymer and geopolymers reinforced with 0.3, 0.6, and 1.5 wt% MWCNTs. XRD, FTIR, and solid-state NMR were implemented to study the chemical influence of MWCNTs. Then, we characterized the dispersion state and microstructure. We implemented scratch testing to evaluate the fracture behavior at the microscale. We also investigated the mechanical behavior, including the indentation hardness and indentation modulus using statistical analyses. Combining the indentation results for chemical characterization, dispersion, microstructure, fracture toughness, mechanical properties, and fresh state rheology characterization, the following conclusions can be derived:

- 1. For dispersion state, the average size of 0.3, 0.6, and 1.5 wt% MWCNTs geopolymers were 5.4 μ m², 6.6 μ m², and 8.9 μ m² respectively, which can be considered well dispersed.
- 2. NMR analysis showed that MWCNTs decreased Q⁴(Al2) but increased the fraction of Q⁴(Al3), suggesting that MWCNTs accelerated the geopolymerization reaction. MWCNTs preserved the amorphous state of geopolymers by XRD results. MWCNTs connected the pore structure, and helped the geopolymer matrix denser.
- 3. The fracture toughness of the plain geopolymer was 0.57 *MPa.*√*m*. A 10.5% increase was observed with addition of 1.5 wt% MWCNTs. MWCNTs act as bridges and pull-out "fibers" to enhance the fracture toughness of metakaolin-based geopolymers. Bridging effects dominate for 1.5 wt% MWCNTs.
- 4. 0.3 and 0.6 wt% MWCNTs increased the strength and stiffness, for the compensation for fracture toughness while 1.5 wt% MWCNTs increased the fracture toughness but for the compensation for



strength and stiffness. The addition of 0.6 and 1.5 wt% MWCNTs promoted another main phase, in terms of indentation modulus and hardness, which increased from 7.700 GPa (plain geopolymer) to 8.171 GPa (5.30% increase) and 8.114 GPa (4.57% increase) of indentation modulus, respectively. Statistical deconvolution analyses showed that MWCNTs strengthened the geopolymer matrix. The indentation hardness increased from 0.414 GPa (plain geopolymer) to 0.445 GPa (7.49% increase) and 0.436 GPa (5.31% increase), with the addition of 0.6 and 1.5 wt% MWCNTs, respectively.

- 5. An increase in the plastic viscosity and the shear yield stress was observed with the addition of MWCNTs, with the highest being for 1.5 wt% MWCNTs. The fresh state result may explain the increase in porosity for high concentration levels. These results suggest that the plastic viscosity and the shear yield stress can be tailored with the addition of MWCNTs, with important implications for 3-D printing applications.
- Our novel mixing method yielded high-performance metakaolin-based geopolymer nanocomposites when reinforced with high concentration levels of 0.6–1.5 wt% MWCNTs.

Acknowledgements

This material is based upon work supported by the National Science Foundation under Grant No. CMMI 1829101. In addition, we would like to acknowledge the Walter P. Murphy Fellowship that supported Jiaxin Chen during her Ph.D. studies at the Department of Civil and Environmental Engineering at Northwestern University. We would also like to acknowledge Raymonde Council and Mairi Rose Glynn. This work made use of the EPIC Facility of Northwestern University's NUANCE Center, which has received support from the Soft and Hybrid Nanotechnology Experimental (SHyNE) Resource (NSF ECCS-1542205); the MRSEC program (NSF DMR-1720139) at the Materials Research Center; the International Institute for Nanotechnology (IIN); the Keck Foundation; and the State of Illinois, through the IIN. This work made use of the Jerome B. Cohen X-Ray Diffraction Facility supported by the MRSEC program of the National Science Foundation (DMR- 1720139) at the Materials Research Center of Northwestern University and the Soft and Hybrid Nanotechnology Experimental (SHyNE) Resource (NSF ECCS-1542205). This work made use of the MatCI Facility supported by the MRSEC program of the National Science Foundation (DMR-1720139) at the Materials Research Center of Northwestern University. This work made use of the Keck-II facility of Northwestern University's NUANCE Center, which has received support from the Soft and Hybrid Nanotechnology Experimental (SHyNE) Resource (NSF ECCS-1542205); the MRSEC program (NSF DMR-1720139) at the Materials Research Center; the International Institute for Nanotechnology (IIN); the Keck Foundation; and the State of Illinois, through the IIN. Moreover, we want to thank BASF for providing the raw metakaolin and Wacker for providing the fumed silica.

Declarations

Conflicts of interest The authors declare that they have no conflicts of interest.

Supplementary Information: The online version contains supplementary material available at https://doi.org/10.1007/s10853-021-06547-0.

References

- [1] Davidovits J (1991) Geopolymers. J Therm Anal 37:1633–1656. https://doi.org/10.1007/bf01912193
- [2] Norton MG, Provis JL (2020) 1000 at 1000: Geopolymer technology—the current state of the art. J Mater Sci 55:13487–13489. https://doi.org/10.1007/s10853-020-04990-7
- [3] Ribero D, Kriven WM (2016) Properties of Geopolymer composites reinforced with basalt chopped strand mat or woven fabric. J Am Ceram Soc 99:1192–1199. https://doi. org/10.1111/jace.14079
- [4] Duxson P, Fernández-Jiménez A, Provis JL et al (2007) Geopolymer technology: the current state of the art. J Mater Sci 42:2917–2933. https://doi.org/10.1007/s10853-006-063 7-z.
- [5] Bernal SA, Rodri ED, Provis JL, Delvasto S (2012) Activation of metakaolin / slag blends using alkaline solutions based on chemically modified silica fume and rice husk ash. Waste Biomass Valor 3:99–108. https://doi.org/10.1007/s12 649-011-9093-3



- [6] Lecomte I, Henrist C, Li M et al (2006) (Micro)-structural comparison between geopolymers, alkali-activated slag cement and Portland cement. J Eur Ceram Soc 26:3789–3797. https://doi.org/10.1016/j.jeurceramsoc.2005. 12.021
- [7] Li J, Zhang W, Li C, Monteiro PJM (2020) Eco-friendly mortar with high-volume diatomite and fly ash: Performance and life-cycle assessment with regional variability. J Clean Prod 261:121224. https://doi.org/10.1016/j.jclepro.2020. 121224
- [8] Li J, Zhang W, Li C, Monteiro PJM (2019) Green concrete containing diatomaceous earth and limestone: workability, mechanical properties, and life-cycle assessment. J Clean Prod 223:662–679. https://doi.org/10.1016/j.jclepro.2019.03 .077
- [9] Rocha S, Dias DP, César F et al (2018) Metakaolin-based geopolymer mortars with different alkaline activators. Constr Build Mater 178:453–461. https://doi.org/10.1016/j.conbuild mat.2018.05.172
- [10] Mendes B, Klaus I, José A et al (2021) Assessment of mechanical and microstructural properties of geopolymers produced from metakaolin, silica fume, and red mud. Int J Appl Ceram Technol 18:262–274. https://doi.org/10.1111/ij ac.13635
- [11] Němeček J, Šmilauer V, Kopecký L (2011) Nanoindentation characteristics of alkali-activated aluminosilicate materials. Cem Concr Compos 33:163–170. https://doi.org/10.1016/j. cemconcomp.2010.10.005
- [12] Fernandez-Jimenez A, García-Lodeiro I, Palomo A (2007) Durability of alkali-activated fly ash cementitious materials. J Mater Sci 42:3055–3065. https://doi.org/10.1007/s10853-006-0584-8
- [13] Shi C, Roy D, Krivenko P (2003) Alkali-activated cements and concretes. CRC Press, London,. https://doi.org/10.1201/ 9781482266900
- [14] Wallah SE, Rangan BV (2006) Low-calcium fly ash-based geopolymer concrete: long-term properties. Res Rep GC
- [15] Provis JL, van Deventer JSJ (2009). Geopolymers: structures, processing, properties and industrial applications. 1st ed., Woodhead Publishing Ltd
- [16] Saafi M, Andrew K, Tang PL et al (2013) Multifunctional properties of carbon nanotube/fly ash geopolymeric nanocomposites. Constr Build Mater 49:46–55. https://doi. org/10.1016/j.conbuildmat.2013.08.007
- [17] Tay YWD, Panda B, Paul SC et al (2017) 3D printing trends in building and construction industry: a review. Virtual Phys Prototyp 12:261–276. https://doi.org/10.1080/17452759.20 17.1326724
- [18] Panda B, Unluer C, Tan MJ (2018) Investigation of the rheology and strength of geopolymer mixtures for extrusion-

- based 3D printing. Cem Concr Compos 94:307–314. https://doi.org/10.1016/j.cemconcomp.2018.10.002
- [19] Su Z, Hou W, Sun Z (2020) Recent advances in carbon nanotube-geopolymer composite. Constr Build Mater 252:118940. https://doi.org/10.1016/j.conbuildmat.2020. 118940
- [20] Senatov FS, Niaza KV, Stepashkin AA, Kaloshkin SD (2016) Low-cycle fatigue behavior of 3d-printed PLA-based porous scaffolds. Compos Part B Eng 97:193–200. https://d oi.org/10.1016/j.compositesb.2016.04.067
- [21] Akono A (2020) Fracture behavior of metakaolin-based geopolymer reinforced with carbon nanofibers. Int J Ceram Eng Sci 2:234–242. https://doi.org/10.1002/ces2.10060
- [22] Chiappone A, Roppolo I, Naretto E et al (2017) Study of graphene oxide-based 3D printable composites: effect of the in situ reduction. Compos Part B Eng 124:9–15. https://doi. org/10.1016/j.compositesb.2017.05.049
- [23] Dul S, Fambri L, Pegoretti A (2016) Fused deposition modelling with ABS-graphene nanocomposites. Compos Part A Appl Sci Manuf 85:181–191. https://doi.org/10.1016/ j.compositesa.2016.03.013
- [24] Han Y, Wang FK, Wang H et al (2018) High-strength boehmite-acrylate composites for 3D printing: reinforced filler-matrix interactions. Compos Sci Technol 154:104–109. https://doi.org/10.1016/j.compscitech.2017.10.026
- [25] Chen Y, Mao J, Wu J (2018) Microwave transparent cross-linked polystyrene nanocomposites with enhanced high voltage resistance via 3D printing bulk polymerization method. Compos Sci Technol 157:160–167. https://doi.org/10.1016/j.compscitech.2018.01.041
- [26] Nguyen QT, Ngo T, Tran P et al (2016) Fire performance of prefabricated modular units using organoclay/glass fibre reinforced polymer composite. Constr Build Mater 129:204–215. https://doi.org/10.1016/j.conbuildmat.2016.10 100
- [27] Dresselhaus MS, Dresselhaus G, Avouris P (Eds.) (2000) Carbon nanotubes: synthesis, structure, properties, and applications. Springer, Berlin
- [28] Huang X, Liang W, Zhang S (2011) Radial corrugations of multi-walled carbon nanotubes driven by inter-wall nonbonding interactions. Nanoscale Res Lett 6:1–6. https://doi. org/10.1007/s11671-010-9801-0
- [29] da Luz G, Gleize PJP, Batiston ER, Pelisser F (2019) Effect of pristine and functionalized carbon nanotubes on microstructural, rheological, and mechanical behaviors of metakaolin-based geopolymer. Cem Concr Compos 104:103332. https://doi.org/10.1016/j.cemconcomp.2019.05.
- [30] Chougan M, Hamidreza Ghaffar S, Jahanzat M et al (2020) The influence of nano-additives in strengthening mechanical



- performance of 3D printed multi-binder geopolymer composites. Constr Build Mater 250:118928. https://doi.org/10.1016/j.conbuildmat.2020.118928
- [31] Ngo TD, Kashani A, Imbalzano G et al (2018) Additive manufacturing (3D printing): a review of materials, methods, applications and challenges. Compos Part B Eng 143:172–196. https://doi.org/10.1016/j.compositesb.2018.02 .012
- [32] Abbasi SM, Ahmadi H, Khalaj G, Ghasemi B (2016) Microstructure and mechanical properties of a metakaolinitebased geopolymer nanocomposite reinforced with carbon nanotubes. Ceram Int 42:15171–15176. https://doi.org/10.1 016/i.ceramint.2016.06.080
- [33] Yuan J, He P, Jia D et al (2017) In situ processing of MWCNTs/leucite composites through geopolymer precursor. J Eur Ceram Soc 37:2219–2226. https://doi.org/10.1016/j.je urceramsoc.2017.01.008
- [34] Khayamdar M, Khoramishad H (2021) The effect of metallic fiber geometry and multi-walled carbon nanotubes on the mechanical behavior of aluminum fiber-reinforced composite adhesive joints. Proc Inst Mech Eng Part L J Mater Des Appl 235(5):949–957. https://doi.org/10.1177/ 1464420720981404
- [35] Khoramishad H, Zarifpour D (2018) Fracture response of adhesive joints reinforced with aligned multi-walled carbon nanotubes using an external electric field. Theor Appl Fract Mech 98:220–229.
- [36] Ashofteh RS, Khoramishad H (2019) The influence of hygrothermal ageing on creep behavior of nanocomposite adhesive joints containing multi-walled carbon nanotubes and graphene oxide nanoplatelets. Int J Adhes Adhes 94:1–12. https://doi.org/10.1016/j.ijadhadh.2019.03.017
- [37] Khoramishad H, Khayamdar M (2016) Toughening epoxy adhesives with multi-walled carbon nanotubes. J Adhesion 94. https://doi.org/10.1080/00218464.2016.1224184
- [38] Gholami R, Khoramishad H, da Silva LFM (2020) Glass fiber-reinforced polymer nanocomposite adhesive joints reinforced with aligned carbon nanofillers. Compos Struct 253:112814. https://doi.org/10.1016/j.compstruct.2020. 112814
- [39] Chen J, Akono AT (2020) Influence of multi-walled carbon nanotubes on the hydration products of ordinary Portland cement paste. Cem Concr Res 137:106197. https://doi.org/ 10.1016/j.cemconres.2020.106197
- [40] Rovnaník P, Šimonová H, Topolář L et al (2016) Effect of carbon nanotubes on the mechanical fracture properties of fly ash geopolymer. Procedia Eng 151:321–328. https://doi.org/ 10.1016/j.proeng.2016.07.360
- [41] Lizcano M, Kim HS, Basu S, Radovic M (2012) Mechanical properties of sodium and potassium activated metakaolin-

- based geopolymers. J Mater Sci 47:2607–2616. https://doi. org/10.1007/s10853-011-6085-4
- [42] Zhang P, Wang K, Wang J et al (2020) Mechanical properties and prediction of fracture parameters of geopolymer/alkaliactivated mortar modified with PVA fiber and nano-SiO2. Ceram Int 46:20027–20037. https://doi.org/10.1016/j.ceram int.2020.05.074
- [43] Khater HM, Abd El Gawaad HA (2016) Characterization of alkali activated geopolymer mortar doped with MWCNT. Constr Build Mater 102:329–337. https://doi.org/10.1016/j.conbuildmat.2015.10.121
- [44] Chen X, Mondal P (2020) Effects of NaOH amount on condensation mechanism to form aluminosilicate, case study of geopolymer gel synthesized via sol-gel method. J Sol-Gel Sci Technol 96:589–603. https://doi.org/10.1007/s10971-02 0-05360-6
- [45] Pegel S, Pötschke P, Villmow T et al (2009) Spatial statistics of carbon nanotube polymer composites. Polymer Guildf 50:2123–2132. https://doi.org/10.1016/j.polymer.2009.02. 030
- [46] ASTM International: ASTM C20-00(2015), standard test methods for apparent porosity, water absorption, apparent specific gravity, and bulk density of burned refractory brick and shapes by boiling water. https://www.astm.org/Standard s/C20.htm
- [47] Théréné F, Keita E, Nael-Redolfi J, Boustingorry P, Bonafous L, Roussel N (2020) Water absorption of recycled aggregates: Measurements, influence of temperature and practical consequences. Cem Concr Res 137:106196–106204
- [48] Abdel-Ghani NT (2014) Individual and competitive adsorption of phenol and nickel onto multiwalled carbon nanotubes. J Adv Res. https://doi.org/10.1016/j.jare.2014.06. 001
- [49] Atchudan R, Pandurangan A, Joo J (2015). Effects of nanofillers on the thermo-mechanical properties and chemical resistivity of epoxy nanocomposites. https://doi.org/10. 1166/jnn.2015.9706
- [50] Nie P, Min C, Song HJ, Chen X, Zhang Z, Zhao K (2016). Preparation and tribological properties of polyimide / car-boxyl-functionalized preparation and tribological properties of polyimide/carboxyl- functionalized multi-walled carbon nanotube nanocomposite films under seawater lubrication. https://doi.org/10.1007/s11249-015-0476-7
- [51] Oliver WC, Pharr GM (1992) An improved technique for determining hardness and elastic modulus using load and displacement sensing indentation experiments. J Mater Res 7:1564–1583. https://doi.org/10.1557/JMR.1992.1564
- [52] Sorelli L, Constantinides G, Ulm FJ, Toutlemonde F (2008) The nano-mechanical signature of ultra high performance



- concrete by statistical nanoindentation techniques. Cem Concr Res 38:1447–1456. https://doi.org/10.1016/j.cemconres.2008.09.002
- [53] Akono AT, Randall NX, Ulm FJ (2012) Experimental determination of the fracture toughness via microscratch tests: application to polymers, ceramics, and metals. J Mater Res 27:485–493. https://doi.org/10.1557/jmr.2011.402
- [54] Akono AT, Ulm FJ (2014) An improved technique for characterizing the fracture toughness via scratch test experiments. Wear 313:117–124. https://doi.org/10.1016/j.wear.2 014.02.015
- [55] Kendall AK, Howard AJ, Birchall JD et al (1983) The relation between porosity, microstructure and strength, and the approach to advanced cement-based materials and discussion, Philos Trans Royal Soc London. Ser A Math and Phys Sci A310:139–153
- [56] Rice RW (1999) Effects of amount, location, and character of porosity on stiffness and strength of ceramic fiber composites via different processing. J Mater Sci 34:2769–2772. https://doi.org/10.1023/A:1004606612294
- [57] Akono AT, Koric S, Kriven WM (2019) Influence of pore structure on the strength behavior of particle- and fiber-reinforced metakaolin-based geopolymer composites. Cem Concr Compos 104:103361. https://doi.org/10.1016/j.cemc oncomp.2019.103361
- [58] Nash SG (2000) A survey of truncated-Newton methods. J Comput Appl Math 124:45–59. https://doi.org/10.1016/S 0377-0427(00)00426-X
- [59] Michie D (1968) "Memo" functions and machine learning. Nature 218:19–22. https://doi.org/10.1038/218019a0
- [60] Akono A, Kabir P (2016) Nano-Scale Characterization of Organic-Rich Shale via Indentation Methods, New frontiers in oil and gas exploration. New Front Oil Gas Explor 40124. https://doi.org/10.1007/978-3-319-40124-9
- [61] Constantinopoulos C, Titsias MK, Likas A (2006) Bayesian feature and model selection for Gaussian mixture models. IEEE Trans Pattern Anal Mach Intell 28:1013–1018. https://doi.org/10.1109/TPAMI.2006.111
- [62] Rasmussen CE (2000) The infinite Gaussian mixture model. Adv Neural Inf Process Syst 554–559
- [63] Chellappa R, Veeraraghavan A, Ramanathan N (2009) Gaussian mixture models. Encycl Biom 659–663.
- [64] Vila JP, Schniter P (2013) Expectation-maximization Gaussian-mixture approximate message passing. IEEE Trans Signal Process 61:4658–4672. https://doi.org/10.1109/TSP. 2013.2272287
- [65] Lee WKW, Van Deventer JSJ (2003) Use of infrared spectroscopy to study geopolymerization of heterogeneous amorphous aluminosilicates. Langmuir 19:8726–8734. https://doi.org/10.1021/la026127e

- [66] Rees CA, Provis JL, Lukey GC, Van Deventer JSJ (2007) In situ ATR-FTIR study of the early stages of fly ash geopolymer gel formation. Langmuir 23:9076–9082. http s://doi.org/10.1021/la701185g
- [67] Davidovits, J. (2015) Geopolymer chemistry and applications. 5-th ed. Geopolymer Institute, Saint-Quentin, France
- [68] Zhang DW, Min Wang D, Lin XQ, Zhang T (2018) The study of the structure rebuilding and yield stress of 3D printing geopolymer pastes. Constr Build Mater 184:575–580. https://doi.org/10.1016/j.conbuildmat.2018.06 .233
- [69] Archez J, Texier-mandoki N, Bourbon X et al (2021) Shaping of geopolymer composites by 3D printing. J Build Eng 34:101894. https://doi.org/10.1016/j.jobe.2020.101894
- [70] Panda B, Unluer C, Tan MJ (2019) Extrusion and rheology characterization of geopolymer nanocomposites used in 3D printing. Compos Part B Eng 176:107290. https://doi.org/10. 1016/j.compositesb.2019.107290
- [71] Chen S, Wu C, Yan D (2019) Binder-scale creep behavior of metakaolin-based geopolymer. Cem Concr Res 124:105810. https://doi.org/10.1016/j.cemconres.2019.105810
- [72] Si R, Guo S, Dai Q, Wang J (2020) Atomic-structure, microstructure and mechanical properties of glass powder modified metakaolin-based geopolymer. Constr Build Mater 254:119303. https://doi.org/10.1016/j.conbuildmat.2020. 119303
- [73] Yan S, Zhang F, Li H, Gao B, Xing P, He P, Jia D, (2020) Synthesis and mechanical properties of lightweight hybrid geopolymer foams reinforced with carbon nanotubes. pp 2335–2345. https://doi.org/10.1111/ijac.13543
- [74] Zou B, Jian S, Korayem AH et al (2014) Effect of ultrasonication energy on engineering properties of carbon nanotube reinforced cement pastes. Carbon N Y 85:212–220. h ttps://doi.org/10.1016/j.carbon.2014.12.094
- [75] Zhan M, Pan G, Zhou F et al (2020) In situ-grown carbon nanotubes enhanced cement-based materials with multifunctionality. Cem Concr Compos 108:103518. https://doi. org/10.1016/j.cemconcomp.2020.103518
- [76] Chen X, Kim E et al (2020) Quantitative correlation between the degree of reaction and compressive strength of Metakaolin-based geopolymers. Materials 13:5784. https://doi.or g/10.3390/ma13245784
- [77] Tsai Y, Hanna JV, Lee Y et al (2010) Journal of solid state chemistry solid-state nmr study of geopolymer prepared by sol-gel chemistry. J Solid State Chem 183:3017–3022. h ttps://doi.org/10.1016/j.jssc.2010.10.008
- [78] Duxson P, Provis JL, Lukey GC, et al (2005) Si NMR study of structural ordering in aluminosilicate geopolymer gels, pp 3028–3036



- [79] Sankar K, Sutrisno A, Kriven WM (2019) Slag-fly ash and slag-metakaolin binders: part II-Properties of precursors and NMR study of poorly ordered phases. J Am Ceram Soc 102:3204–3227. https://doi.org/10.1111/jace.16224
- [80] Gupta R, Bhardwaj P, Deshmukh K, et al (2019) Development and characterization of inorganic-organic (Si-O-Al) hybrid geopolymeric precursors via solid state method, pp 221–232
- [81] Samuel DM, Sutrisno A, Kriven W, (2021) Relative importance of Al (V) and reinforcement to the flexural

- strength of geopolymer composites, pp 3452–3460. https://doi.org/10.1111/jace.17656
- [82] Provis JL (2006) Modelling the formation of geopolymers. Thesis 44:8–10

Publisher's Note Springer Nature remains neutral with regard to jurisdictional claims in published maps and institutional affiliations.

